Transition of Macrophages to Fibroblast-like Cells in Healing Myocardial Infarction

*Nezam Haider[a,b] MD PhD, *Lisardo Boscá[c,d] PhD, *H. Reinier Zandbergen[e] MD PhD, Jason C. Kovacic[a] MD PhD, Navneet Narula[f] MD PhD, Silvia González-Ramos[c,d] PhD, María Fernandez-Velasco[d,g] PhD, Sudhanshu Agrawal[h] SCYM(ASPC), Marta Paz-García[c] MSc, Sudhir Gupta[h] MD PhD, Kristine DeLeon-Pennell[i] PhD, Valentin Fuster[a,j] MD PhD, Borja Ibañez[d,j,k] MD PhD, Jagat Narula[a] MD PhD
*NH, LB and HRZ contributed equally to the manuscript

[a]Zena and Michael A. Wiener Cardiovascular Institute, Icahn School of Medicine at Mount Sinai, New York, New York.
[b]Division of Vascular Surgery. University of Arizona. Tucson, AZ
[c]Instituto de Investigaciones Biomédicas Alberto Sols (CSIC-UAM), Arturo Duperier 4, Madrid, Spain.
[d]Centro de Investigación Biomédica en Red de Enfermedades Cardiovasculares, Melchor Fernández Almagro, Madrid, Spain.
[e]Department of Cardiothoracic Surgery, Amsterdam University Medical Center, Amsterdam, Netherlands.
[f]Department of Pathology, New York University Langone Medical Center, New York, USA.
[g]Instituto de Investigación Biomédica LaPaz, Paseo de la Castellana, Madrid, Spain.
[h]Division of Basic and Clinical Immunology, University of California, Irvine, California
[i]Division of Cardiology, Medical University of South Carolina, Ralph H. Johnson Veterans Affairs Medical Center, Charleston, SC
[j]Centro Nacional de Investigaciones Cardiovasculares (CNIC), Madrid, Spain.
[k]Instituto de Investigación Sanitaria-Fundación Jiménez Díaz, Madrid, Spain.

Brief title: *Macrophage-Fibroblast Interplay in Healing MI*

Funding: This work was supported by grants SAF2017-82436R and RTC2017-6283 from MINEICO, S2017/BMD-3686 from Comunidad de Madrid, CIVP18A3864 from Fundación Ramón Areces and Ciberehd (funded by the Instituto de Salud Carlos III) and Fondos FEDER. The Biomedical Laboratory Research and Development Service of the Veterans Affairs Office of Research and Development Award IK2BX003922 to KYD-P.

Conflict of Interest: Authors declare no competing interests.
Acknowledgments: The authors acknowledge Ms Verónica Terrón and Ana Gómez-Sáez for valuable help in the manipulation of the animals and protein assays.

Address for correspondence:
Lisardo Boscá, PhD
Instituto de Investigaciones Biomédicas Alberto Sols (CSIC-UAM)
Arturo Duperier 4
Madrid, Spain
Telephone: +34 914972747
Fax: +34 914972746
E-mail: lbosca@iib.uam.es
Twitter: @LubbDup | @Borjaibanez1 | @CNIC_CARDIO

ABSTRACT

Background: Macrophages and fibroblasts are two major cell types involved in healing after myocardial infarction (MI), contributing to myocardial remodeling and fibrosis. Post-MI fibrosis progression is characterized by a decrease in cardiac macrophage content.

Objectives: This study explores the potential of macrophages to express fibroblast genes and the direct role of these cells in post-MI cardiac fibrosis.

Methods: Prolonged *in vitro* culture of human macrophages was used to evaluate the capacity to express fibroblast markers. Infiltrating cardiac macrophages was tracked *in vivo* after experimental MI of LysM($Cre^{/+}$);ROSA26($EYFP^{/+}$) transgenic mice. The expression of Yellow Fluorescent Protein (YFP) in these animals is restricted to myeloid lineage allowing the identification of macrophage-derived fibroblasts. The expression in YFP-positive cells of fibroblast markers was determined in myocardial tissue sections of hearts from these mice after MI.

Results: Expression of the fibroblast markers type I collagen, prolyl-4-hydroxylase, fibroblast specific protein-1 and fibroblast activation protein was evidenced in YFP-positive cells in the heart after MI. The presence of fibroblasts after MI was evaluated in the hearts of animals after depletion of macrophages with clodronate liposomes. This macrophage depletion significantly reduced the number of $Mac3^{+}Col1A1^{+}$ cells in the heart after MI.

Conclusions: The data provide both *in vitro* and *in vivo* evidence for the ability of macrophages to transition and adopt a fibroblast-like phenotype. Therapeutic manipulation of this macrophage-fibroblast transition may hold promise for favorably modulating the fibrotic response after MI and after other cardiovascular pathologic processes.

CONDENSED ABSTRACT

This study evaluates the ability of cardiac macrophages after myocardial infarction, to express genes and proteins associated to the fibroblast phenotype, focused in the progression of adverse cardiac fibrosis. Using transgenic mice in which the myeloid lineage can be tracked through the expression of the green/yellow fluorescent protein EYFP we showed the presence of fibroblast-like cells of monocytic origin. This transition was characterized by the co-expression of EYFP and the fibroblast proteins type I collagen, prolyl-4-hydroxylase, fibroblast specific protein-1 and α-smooth muscle actin. Additionally, cardiac cells expressing macrophage markers and fibroblast genes were identified.

Keywords: macrophage/fibroblast-like transition; infiltration; cardiac fibroblast; myocardial infarction; myeloid tracers; fibroblast markers.

Abbreviations:

LVEF: left ventricular ejection fraction

MI: myocardial infarction

INTRODUCTION

Myocardial healing after myocardial infarction (MI) is accomplished by replacement fibrosis in the damaged region, and interstitial fibrosis takes place in the remote areas towards adverse ventricular remodeling. The collagen is produced by myofibroblasts, with infiltrating macrophages further facilitating this process (1,2). Macrophages infiltrate in large number at the site of injury after MI in human and in experimental animal models (3). These macrophages aid in the process of myocardial healing and assume multiple roles at different stages, depending on their origin whether infiltrating *or* resident (3,4). This involves removal of dead necrotic and apoptotic cells, regulation of fibroblast/myofibroblast function and ultimately wound resolution. Macrophages and fibroblasts are 2 major cell types involved in myocardium healing, and often lead to adverse myocardial remodeling and fibrosis (1,2,5).

It is well established that differentiated cells in various circumstances change their phenotype and transition into other cell types in adult tissues. For example, endothelial cells differentiate into beating cardiomyocytes when co-cultured with neonatal rat cardiomyocytes or injected into the post-ischemic adult mouse heart (6). Studies have demonstrated the trans-differentiation of macrophages into endothelial cells (7,8) and conversion of preadipocytes into macrophages (9). In fibrosis of many tissues, the presence of fibroblasts derive from epithelial cells (10). Macrophages are versatile cells and respond aptly to the environmental cues of the site of their localization (3,4,11-13). We hypothesized that dynamic microenvironment changes during myocardial healing which are conducive for fibrosis can induce fibroblast-like phenotype in macrophages present at the site of infarct. This macrophage to fibroblast-like transition might augment cardiac fibrosis by collagen deposition.

In this study, we have explored the potential of macrophages to convert into collagen producing fibroblast-like cells, in the absence of any other accessory cells. Since components

of the renin–angiotensin–aldosterone system exert a significant influence on cardiac, renal and hepatic fibrosis (14), we also evaluated the effect of aldosterone, angiotensin II and hypoxia on macrophage to fibroblast-like transition *in vitro*. Moreover, we looked for a similar macrophage to fibroblast differentiation in a mouse model of MI. Fibroblast classic markers, including type I collagen (COL1A1), prolyl-4-hydroxylase (P4H), fibroblast specific protein-1 (FSP1/S100A4), fibroblast activation protein (FAP) and α-smooth muscle actin (α-SMA) were sought to evaluate this macrophage to fibroblast-like transition (15-17).

EXPERIMENTAL PROCEDURES (Supplementary Appendix)

Peripheral blood derived CD14$^+$ monocytes.

Monocytes were obtained from human peripheral blood buffy coats (each from 50 ml of blood from healthy donors) by Ficoll-Paque centrifugation. Subsequently, $CD14^+$ monocytes were isolated using EasySep Human CD14 Positive Selection Kit, according to the manufacturer's instructions. These cells were grown in RPMI 1640 medium (Mediatech, Manassas, VA) supplemented with 10% fetal bovine serum, 100 units/ml penicillin, 100 µg/ml streptomycin, and 2 mM L-glutamine. Cells were incubated at 1–$2x10^6$ cells per well in 12 well tissue culture plates for 24 hours at 37°C and 5% CO_2. Finally, $CD14^+$ monocytes were treated with 10 ng/ml of PMA to differentiate monocytes into macrophages. The individual monocyte-derived cultures used in these experiments were obtained from separate donors at different times.

Preparation of cell extracts.

Whole-cell lysates were prepared by lysing cells in lysis buffer (10 mM Tris; pH 7.5, 150 mM NaCl, 1% NP-40, 200 µg/ml leupeptin, 10 µg/ml aprotinin, 1 mM phenylmethylsulfonyl fluoride, 10 mM NaF, 1 mM Na_3VO_4, 1 mM dithiothreitol). Protein concentration was measured using a Bio-Rad DC protein assay kit (Bio-Rad Laboratories, Hercules, CA). Equal amounts of each protein samples for each assay (10-50 micrograms)

were separated by 10% SDS-polyacrylamide gels and electroblotted to nitrocellulose membrane by Tran-Blot SD, Semi-Dry Transfer Cell (Bio-Rad). Membranes were then either incubated with rabbit polyclonal COL1A1 antibody, anti-P4H-β mouse monoclonal antibody, anti-tenascin-C antibody, anti-transgelin antibody, anti-vimentin antibody and, after washing, with horseradish peroxidase-conjugated goat anti-mouse or anti-rabbit secondary antibodies. Immunoreactive bands were detected with ECL solution (GE Healthcare Life Sci.).

Mice.

LysM(Cre$^{/+}$);ROSA26(EYFP$^{/+}$) mice were used to track the fate of macrophages in an MI and heart failure model. LysM(Cre$^{/+}$);ROSA26(EYFP$^{/+}$) mice were generated by crossing the LysM-Cre mouse line (Jackson Laboratory, Bar Harbor, ME; strain 004781) with the R26R-EYFP line (Jackson Laboratory; strain 006148). LysM-Cre mice express Cre in myeloid cells due to a targeted insertion in their endogenous M lysozyme locus. The R26R-EYFP mouse is a Cre-dependent YFP reporter strain (R26R) produced by targeted insertion of EYFP preceded by a loxP flanked (floxed) transcriptional termination sequence (tpA) into the ROSA26 locus. The R26R allele terminates transcription prematurely, but when crossed with LysMCre mice, the Cre-mediated excision of the floxed termination sequence in myeloid cells leads to YFP expression. LysM(Cre$^{/+}$); ROSA26(EYFP$^{/+}$) mice are useful for myeloid cell tracking in vivo and exhibit specific and efficient expression of YFP protein in 83–98% mature macrophages and 100% granulocytes (18). In addition to the LysM(Cre$^{/+}$);ROSA26(EYFP$^{/+}$) mouse strain, two-month-old male wild type mice (C57BL6/J mice; Jackson Laboratory; strain 000664) were used for MI in the same way. When animals were depleted of resident macrophages, clodronate liposomes were administered 2 days prior to MI following the protocol provided by the supplier (Sigma-Aldrich). When animals were treated with inhibitors of glycolysis (3PO) and glutaminase (C968), the drugs were dissolved in dimethylacetamide

(DMA) and administered i.p. at 50 mg/kg body weight at day -1, and for 3 consecutive days after MI. Controls received equivalent amounts of DMA. All animal studies were performed in accordance with the NIH Guidelines for the Use of Laboratory Animals and were approved by the institutional and national boards for laboratory animal research.

Experimental MI and heart failure in mice.

After anesthesia with intramuscular ketamine (80 mg/kg) and xylazine (15 mg/kg), mice were anesthetized with inhalation of 5% isoflurane and maintained with inhalation of 1-3% isoflurane. Mice were intubated and ventilation was maintained with a Harvard rodent positive-pressure respirator at a respiratory rate of 130/min. Mice were immobilized on a heating pad and subjected to left-sided thoracotomy between the third and fourth intercostal space. MI was induced by permanent ligation of the left anterior descending coronary artery (19). After opening the pericardium, ligation of LAD was made 1 mm under the left atrial appendage using a silk 7/0 suture. MI was confirmed by changes of the affected area from bright red to pale. The left thorax incision was closed with 6.0 monocryl suture. The small pectoral muscle was moved back to its original place and the skin was closed with 6.0 silk sutures. Sham operated mice underwent a similar surgical procedure except without ligation of the LAD (20). Functional parameters were determined by echocardiography/electrocardiography (Vevo 2100 System, VisualSonics, Toronto, Canada). One week to 8 weeks post-MI hearts were harvested for analysis. The heart rate, the PR and QRS intervals (in milliseconds), the E/A ratio of peak velocity of blood flow from gravity in early diastole (the E-wave) to peak velocity flow in late diastole caused by atrial contraction (the A-wave) and the left ventricular ejection fraction (LVEF) were determined.

Immunohistochemical analysis of myocardial tissue sections.

At designated time points, hearts were harvested for histology. At each study, time point hearts were excised and washed with PBS. Hearts were fixed in 4% paraformaldehyde in PBS followed by 30% sucrose and embedded in Tissue-Tek OCT compound. Myocardial serial tissue cryosections (5-7 µm) were prepared for immunofluorescence analysis. For immunostaining, tissue sections were rinsed in PBS, unspecific binding sites were blocked with 1% BSA in PBS for 60 min at room temperature, and primary antibodies (1:100 prediluted in blocking solution) were applied for 1 h at room temperature. For double labeling experiments, sections were washed three times with PBS and the second primary antibody was applied for 1 h at room temperature. Antigen-antibody complexes were visualized using fluorochrome (Alexa 484 and 594)-conjugated secondary antibodies (Invitrogen; prediluted in blocking solution). Photomicrographs were taken using a Leica DMIRE2 fluorescence microscope and Compix digital imaging software.

Statistical analysis

Results are presented as mean ± SEM. Statistical significance was estimated with Student's t test. Grubbs test was used to determine and discard outliers. Differences with values of $p<0.05$ were considered statistically significant.

RESULTS

***In vitro* expression of fibroblast markers in activated human macrophages.**

a. Morphological changes during the transition of macrophages to fibroblast-like cells.

Purified $CD14^+$ monocytes from peripheral blood were maintained in complete RPMI 1640 medium (Fig. 1A,a-b). $CD14^+$ cells were treated with 10nM PMA to achieve differentiation into macrophages. After overnight treatment with PMA, $CD14^+$ cells attached to the culture plate, increased in size and acquired a macrophage-like morphology (Fig. 1A,c). No changes were observed in $CD14^-$ cells with identical PMA treatment (data not

shown). PMA-treated $CD14^+$ cells were maintained in culture for up to 14 weeks without any further addition of PMA or growth factors; this was the endpoint of our experiment. During this period, activated macrophages assumed an elongated and spindle shaped morphology, and tended to orient end-to-end or parallel to each other (Fig. 1A,d). Similar results were obtained in PMA differentiated $CD14^+$ cells that were maintained in the presence of aldosterone or angiotensin II (Fig. 1A,e-f).

b. Expression of fibroblast markers during the transition of macrophages to fibroblast-like cells.

We evaluated the expression of known fibroblast markers FSP1/S100A4, α-SMA, P4H and collagen I in activated macrophages by immunofluorescence staining. Fig. 1B shows the expression of FSP1 in macrophages 1-12 weeks after activation; FSP1 was not detectable after one-week culture (Fig. 1B,a-b) but was gradually expressed. Most PMA-activated cells were $FSP1^+$ after 8-12 weeks (Fig. 1B,e-h). The expression profile of α-SMA was similar to that of FSP1. No α-SMA protein was detected in early macrophages (Fig. 1C,a-b), but this gradually increased after 8-12 weeks in culture (Fig. 1C,e-h). P4H (a collagen modifying enzyme) was detected as early as one-week after activation and this expression increased moderately after that for up to twelve weeks (Fig. 1D,a-h). Immunoblot analysis showed a low level of P4H protein in untreated $CD14^+$ monocytes. $COL1A1^+$-cells expression followed the FSP1 and α-SMA pattern (Fig. 1E,a-b). COL1A1 expression increased gradually and 8-12 weeks after activation a large number of COL1A1-positive cells were detected in the culture (Fig. 1E,e-h). Collagen quantification assay also detected secreted collagen in the culture medium (Supplementary Fig. S1). In parallel to increase in the number of $COL1A1^+$-cells, the amount of secreted collagen also gradually increased in the culture medium over a period of 12 weeks.

c. Effect of aldosterone, angiotensin II and hypoxic stress on macrophage to fibroblast-like cell transition.

Aldosterone, angiotensin II and hypoxic stress have been reported to enhance fibrosis *in vivo* but had no effect on the transition of activated macrophages to fibroblast-like cells in culture. Macrophages treated with aldosterone, angiotensin II (Supplementary Fig. S2) or subjected to hypoxia alone or in combination had no effect on COL1A1 protein expression in cells nor in COL1A1 secreted into the culture medium (Supplementary Fig. S3).

Transition of macrophages to fibroblast-like cells in healing mouse heart after myocardial infarction.

a. Cell lineage tracking for transition of macrophages to fibroblast-like cells in LysM(Cre$^{/+}$);ROSA26(EYFP$^{/+}$) transgenic mice.

To circumvent the overlapping of cell markers present in both macrophages and fibroblasts *in vivo* we used LysM(Cre$^{/+}$);ROSA26(EYFP$^{/+}$) transgenic mice (18). In these animals, identification and tracking of cells derived from macrophages after MI is possible due to the permanent expression of the YFP reporter protein in macrophages or different cell types derived from these macrophages. We analyzed serial heart sections obtained after MI by immunofluorescence staining for the presence of cells expressing both YFP and fibroblast markers (FSP1, FAP, COL1A1 and α-SMA). Interestingly, COL1A1 and YFP co-positive cells were present in myocardial sections obtained from 1-week post-MI hearts (Fig. 2A,a-c). Although the COL1A1 staining was less intense than YFP, the number of positive cells was higher. In tissue sections from 6 weeks post-MI, clusters of YFP and intense COL1A1 stained co-positive cells were present (Fig. 2A,d-f). Cells expressing both FSP1 and YFP were also present in 1 and 8 weeks post-MI heart samples (Fig. 2B). Expression of FSP1 progressively increased over a period of time after MI and fitted the reported trajectory of cardiac fibrosis. FAP was expressed in YFP-positive cells in the heart at 6 and 8 weeks post-

MI (Fig. 2C). A large number of cells were positive for α-SMA in 1 and 6 week post-MI heart samples; however, YFP and α-SMA co-positive cells were not observed in the myocardial sections analyzed (Fig. 2D). This is in contrast to *in vitro* results where α-SMA was expressed in macrophages after 4, 8 and 12 weeks of activation.

b. Macrophage depletion reduced the number of Mac3$^+$COL1A1$^+$-cells in healing mouse heart after MI.

Cardiac macrophages were evaluated for fibroblast-like cell transition after MI. Experimental groups of animals treated with clodronate liposomes (for resident macrophage depletion), C968 (glutaminase inhibitor to represses the growth and invasiveness of fibroblasts) and 3PO (PFKFB3 inhibitor targeting the glycolytic flux of proinflammatory macrophages) were compared. Hearts were processed one week after MI for immunostaining. Myocardial transverse sections (5µm) were stained with anti-Mac3 (CD107b) and anti-collagen type I antibodies and nuclei with DAPI. Cells showing co-localization of both markers were counted and presented as percentage of the total number of cells per field (Fig. 3A). The number of Mac3$^+$COL1A1$^+$-cells was significantly reduced (4.6±0.7%) after clodronate treatment *vs.* the untreated control group (8.4±1.6%). Inhibition of inflammatory macrophages with 3PO significantly reduced the number of Mac3$^+$COL1A1$^+$ cells (4.0±0.7%) in treated groups while in mice administered C968 (8.3±0.7) the number of Mac3$^+$COL1A1$^+$-cells remain unchanged (Fig. 3A). The effect of these treatments on functional cardiac parameters was determined in these animals (Fig. 3B-E), The PR interval (ms) exhibited minimal, but statistically significant values in animals depleted of macrophages after clodronate administration or treated with 3PO, suggesting a minor difference in electrical conduction was observed. Indeed, cardiac macrophages contribute to physiological atrioventricular nodal conduction (21). No differences were observed in the

QRS value (Fig. 3B). The ratio of peak velocity blood flow (E/A ratio), the heart rate and the LVEF were similar regardless the treatment of the animals, following MI (Fig. 3C-E).

c. Appearance of CD90$^+$F4/80$^+$ macrophage/fibroblast-like cells in the healing mouse heart after MI.

Cells isolated from the mouse heart after MI and sham operated groups were analyzed by flow cytometry for the presence of macrophage/fibroblast-like cells. Isolated cells were stained with cardiomyocyte (MHC$^+$), macrophage (F4/80$^+$) and fibroblast (CD90$^+$) selective antibodies for flow cytometric analysis and quantification (Fig. 4A,a-b). Infarcted hearts showed an increased number of macrophages and fibroblasts, as well as CD90$^+$F4/80$^+$-cells *vs.* the sham group. The number of F4/80$^+$-cells in heart increased from 5.4±1.7% in sham operated to 14.9±3.4% after MI, while the number of CD90$^+$-cells increased from 0.48±0.41% to 3.4±1.5%. Cells with both macrophage and fibroblast markers (CD90$^+$F4/80$^+$) were increased from 0.17±0.15% to 3.5±1.5% (Fig. 4A,b).

d. Expression of macrophage and fibroblast genes in CD90$^+$F4/80$^+$ cells.

Dual positive CD90$^+$F4/80$^+$-cells were isolated by cell sorting from digested hearts from mice submitted to sham or after MI (Fig. 4B,a). RNA isolated from these cells was analyzed by quantitative Real-Time PCR for the expression of macrophage and fibroblast genes (Fig. 4B,b). CD90$^+$F4/80$^+$-cells were positive for macrophage (*Cd163, Cd68, Ly6C, Csfr1)* and fibroblast (*Tagln, Vim*, *Ddr2* and *Pdgfrb)* transcripts. Macrophage transcripts for *Cd163, Ly6C* were significantly upregulated and the level of *Csfr1* was also higher in isolated CD90$^+$F4/80$^+$-cells post-MI *vs*. controls (sham). The levels of CD163, vinculin, transgelin and tenascin-C RNA (*Cd163, Vcl, Tagln and Tnsc)* and protein levels were also significantly upregulated in CD90$^+$F4/80$^+$-cells from the post-MI heart (Fig. 4B,b-c). These proteins have been associated to post-MI fibroblast-induced fibrosis (22,23). However, the levels of *Ddr2* (with very low expression in these cells) and *Pdgfrb* transcripts were significantly reduced in

$CD90^+F4/80^+$-cells post-MI *vs.* control heart. Krüppel-like factor-4 (KLF4), which plays a key role in regulating phenotypic transitions of SMCs *in vivo* during development and after carotid ligation injury (24,25), was upregulated in $CD90^+F4/80^+$-cells from the post-MI heart, suggesting a phenotypic transition of macrophages to fibroblast-like cells.

DISCUSSION

Transition of monocytes/macrophages into fibroblast-like cells has been reported in different pathologic circumstances (i.e. renal fibrosis (13)), probably due to the plasticity of the myeloid lineage (5,26,27). In addition to this, fibroblasts in different organs during pathological remodeling show considerable phenotypic heterogeneity (28-31). This heterogeneity may be due to their different sources of origin: local tissue resident fibroblasts, progenitor cells, fibrocytes, pericytes and EMT transition of epithelial cells (10). Therefore, the different sources of fibroblasts may dictate the outcome of wound healing and shape the degree of tissue scarring (**Central Illustration)**. During cardiac remodeling after MI, the highly profibrotic microenvironment might induce a fibroblast-like phenotype in infiltrating macrophages, present in large numbers and contributing to healing. These fibroblast-like cells should help accomplish the ongoing process of myocardial replacement fibrosis (2,32). Several shared markers of macrophages and fibroblasts have been previously reported (33). Mouton et al. identified a fibroblast-like macrophage population from the infarct region at day 7 post-MI (34). Similar to our findings, this macrophage population had an upregulation of ECM genes including *Col1a1, Vlc, Tnc, Tagln* and *Postn*. This supports the possibility that cells expressing common macrophage and fibroblast markers represent a specific cell population. To address this possible origin of fibroblasts, we tested the ability of a human macrophages to assume a fibroblast-like phenotype *in vitro*. In this proof of principle study, we identified an emergence of fibroblast-like cells from purified $CD14^+$ human monocytes differentiated into macrophages. Previous studies have suggested a crosstalk between

macrophages and fibroblasts that may represent an additional possibility of differentiation (19,35). The notion of macrophage to fibroblast-like transition was further supported by our results in a transgenic mouse model where YFP-expressing macrophages were tracked and observed to acquire a fibroblast-like phenotype in healing MI.

Macrophages play a crucial role in cardiac fibrosis (1). First, by modulating the number and function of the fibroblasts recruited at the site of infarction, and second, more directly by converting into fibroblast-like cells and depositing collagen and extracellular matrix. The newly converted fibroblasts did not express many fibroblast markers of a conventional fibroblast and may represent a group of pathogenic fibroblasts similar to those identified by other groups (13,15,28,29,32,36). Transcription factor KLF4 has been shown to facilitate phenotypic transition, and its upregulation during the healing phase of mouse myocardium in $CD90^{+}F4/80^{+}$-cells indicates an ongoing macrophage to fibroblast transition (3,24,25). The newly converted pathogenic fibroblasts perhaps lack the control, competence and finesse of a conventional fibroblast in maintaining collagen homeostasis and may engage in uncontrolled deposition of collagen and extracellular matrix. However, the possibility exists that resident macrophages in the heart can also be differentiated into fibroblast-like cells contributing to the known requirement of macrophages to improve cardiac regeneration after MI (1,3).

STUDY LIMITATIONS

The present study is intended to validate the proof-of-concept that macrophages in the heart can express characteristic fibroblast markers after MI, including the capacity to contribute to adverse fibrosis. However, the specific role of resident versus infiltrating macrophages has not been evaluated in terms of the ability to differentiate into fibroblast-like cells. Also, the balance between the beneficial fibrosis following MI and the adverse fibrogenic effects in the course of heart healing, require further in-depth analysis to determine

the exact pathological contribution of the cell-transition described in this work. Finally, the extent of the differentiation process requires quantification in terms of the percentages of cells present in the injured tissue.

CLINICAL PERSPECTIVES

Competency in Medical Knowledge: In survivors of myocardial infarction, transition of macrophages to fibroblasts influences the evolution of myocardial fibrosis and development of heart failure.

Translational Outlook: Specific targeting of pathogenic macrophage transformation to inhibit fibrosis in ways that do not interfere with normal fibroblast function may have therapeutic potential for survivors of myocardial infarction.

REFERENCES

1. Cheng B, Chen HC, Chou IW, Tang TW, Hsieh PC. Harnessing the early post-injury inflammatory responses for cardiac regeneration. J Biomed Sci. 2017;24:7.
2. Frangogiannis NG. Inflammation in cardiac injury, repair and regeneration. Curr Opinion Cardiol 2015;30:240-5.
3. Liao X, Shen Y, Zhang R et al. Distinct roles of resident and nonresident macrophages in nonischemic cardiomyopathy. Proc Natl Acad Sci USA. 2018;115:E4661-E4669.
4. Bonaventura A, Montecucco F, Dallegri F. Cellular recruitment in myocardial ischaemia/reperfusion injury. Eur J Clin Invest 2016;46:590-601.
5. Laurent P, Jolivel V, Manicki P et al. Immune-Mediated Repair: A Matter of Plasticity. Frontiers Immunol 2017;8:454.
6. Condorelli G, Borello U, De Angelis L et al. Cardiomyocytes induce endothelial cells to trans-differentiate into cardiac muscle: implications for myocardium regeneration. Proc Natl Acad Sci USA 2001;98:10733-8.
7. Krenning G, Dankers PY, Jovanovic D, van Luyn MJ, Harmsen MC. Efficient differentiation of CD14+ monocytic cells into endothelial cells on degradable biomaterials. Biomaterials 2007;28:1470-9.
8. Rehman J, Li J, Orschell CM, March KL. Peripheral blood "endothelial progenitor cells" are derived from monocyte/macrophages and secrete angiogenic growth factors. Circulation 2003;107:1164-9.
9. Charriere G, Cousin B, Arnaud E et al. Preadipocyte conversion to macrophage. Evidence of plasticity. J Biol Chem 2003;278:9850-5.

10. Iwano M, Plieth D, Danoff TM, Xue C, Okada H, Neilson EG. Evidence that fibroblasts derive from epithelium during tissue fibrosis. J Clin Invest 2002;110:341-50.

11. Hamerman JA, Aderem A. Functional transitions in macrophages during in vivo infection with Mycobacterium bovis bacillus Calmette-Guerin. J Immunol 2001;167:2227-33.

12. Strutz F, Okada H, Lo CW et al. Identification and characterization of a fibroblast marker: FSP1. J Cell Biol 1995;130:393-405.

13. Wang YY, Jiang H, Pan J et al. Macrophage-to-Myofibroblast Transition Contributes to Interstitial Fibrosis in Chronic Renal Allograft Injury. J Am Soc Nephrol 2017;28:2053-2067.

14. Watanabe T, Barker TA, Berk BC. Angiotensin II and the endothelium: diverse signals and effects. Hypertension. 2005;45:163-9.

15. Kelly T, Huang Y, Simms AE, Mazur A. Fibroblast activation protein-alpha: a key modulator of the microenvironment in multiple pathologies. Internat Rev Cell Mol Biol 2012;297:83-116.

16. Myllyharju J. Prolyl 4-hydroxylases, the key enzymes of collagen biosynthesis. Matrix Biol 2003;22:15-24.

17. Rettig WJ, Garin-Chesa P, Healey JH et al. Regulation and heteromeric structure of the fibroblast activation protein in normal and transformed cells of mesenchymal and neuroectodermal origin. Cancer Res 1993;53:3327-35.

18. Abram CL, Roberge GL, Hu Y, Lowell CA. Comparative analysis of the efficiency and specificity of myeloid-Cre deleting strains using ROSA-EYFP reporter mice. J Immunol Methods 2014;408:89-100.

19. Clancy RM, Kapur RP, Molad Y, Askanase AD, Buyon JP. Immunohistologic evidence supports apoptosis, IgG deposition, and novel macrophage/fibroblast crosstalk in the pathologic cascade leading to congenital heart block. Arthritis Rheumatism 2004;50:173-82.

20. Cuadrado-Berrocal I, Gomez-Gaviro MV, Benito Y et al. A labdane diterpene exerts ex vivo and in vivo cardioprotection against post-ischemic injury: involvement of AKT-dependent mechanisms. Biochem Pharmacol 2015;93:428-39.

21. Hulsmans M, Clauss S, Xiao L et al. Macrophages facilitate electrical conduction in the heart. Cell 2017;169:510-522.e20.

22. Lighthouse JK, Small EM. Transcriptional control of cardiac fibroblast plasticity. J Mol Cell Cardiol 2016;91:52-60.

23. Park WJ, Jeong D, Oh JG. Tenascin-C in cardiac hypertrophy and fibrosis: friend or foe? J Am Coll Cardiol 2017;70:1616-1617.

24. Ghazizadeh Z, Rassouli H, Fonoudi H et al. Transient activation of reprogramming transcription factors using protein transduction facilitates conversion of human fibroblasts toward cardiomyocyte-like cells. Mol Biotech 2017;59:207-220.

25. Liao X, Zhang R, Lu Y et al. Kruppel-like factor 4 is critical for transcriptional control of cardiac mitochondrial homeostasis. J Clin Invest 2015;125:3461-76.

26. Rapino F, Robles EF, Richter-Larrea JA, et al. C/EBPalpha induces highly efficient macrophage transdifferentiation of B lymphoma and leukemia cell lines and impairs their tumorigenicity. Cell Reports 2017;19:1281.

27. Yan D, He Y, Dai J, Yang L, Wang X, Ruan Q. Vascular endothelial growth factor modified macrophages transdifferentiate into endothelial-like cells and decrease foam cell formation. Biosci Reports 2017;37.

28. Sugimoto H, Mundel TM, Kieran MW, Kalluri R. Identification of fibroblast heterogeneity in the tumor microenvironment. Cancer Biol & Therapy 2006;5:1640-6.

29. Di Carlo SE, Peduto L. The perivascular origin of pathological fibroblasts. J Clin Invest 2018;128:54-63.

30. Driskell RR, Watt FM. Understanding fibroblast heterogeneity in the skin. Trends Cell Biol 2015;25:92-9.

31. Sriram G, Bigliardi PL, Bigliardi-Qi M. Fibroblast heterogeneity and its implications for engineering organotypic skin models in vitro. Eur J Cell Biol 2015;94:483-512.

32. Roche PL, Filomeno KL, Bagchi RA, Czubryt MP. Intracellular signaling of cardiac fibroblasts. Comprehensive Physiol 2015;5:721-60.

33. Inoue T, Plieth D, Venkov CD, Xu C, Neilson EG. Antibodies against macrophages that overlap in specificity with fibroblasts. Kidney International 2005;67:2488-93.

34. Mouton AJ, DeLeon-Pennell KY, Rivera Gonzalez OJ et al. Mapping macrophage polarization over the myocardial infarction time continuum. Basic Res Cardiol 2018;113:26.

35. Leinonen JV, Korkus-Emanuelov A, Wolf Y et al. Macrophage precursor cells from the left atrial appendage of the heart spontaneously reprogram into a C-kit+/CD45- stem cell-like phenotype. Int J Cardiol 2016;209:296-306.

36. Kim YB, Yoon YS, Choi YH, Park EM, Kang JL. Interaction of macrophages with apoptotic cells inhibits transdifferentiation and invasion of lung fibroblasts. Oncotarget 2017;8:112297-112312.

FIGURES LEGENDS

Central Illustration. Transition of macrophages to fibroblast-like cells after experimental myocardial infarction. (A) Heart infiltrating myeloid cells from LysM(Cre^{+});ROSA26($EYFP^{+}$) after myocardial infarction acquire a fibroblast-like phenotype that can be tracked with specific cell markers. **(B)** Macrophage depletion after clodronate liposomes administration reduces the percentage of Mac3/COL1A1 double positive cells in the heart following myocardial infarction.

Figure 1. (A) Differentiation of human $CD14^{+}$ peripheral blood monocytes into macrophages. (a) Freshly isolated monocytes. (b) Untreated one-day cultured monocytes. (c) One-day PMA treated monocytes. (d) PMA activated monocytes after 12-weeks. (e) PMA activated and aldosterone-treated monocytes after 12 weeks. (f) PMA activated and angiotensin II-treated monocytes after 12 weeks. Cells were visualized by phase-contrast microscopy. **Expression of FSP1, α-SMA, P4H-β and type1 collagen (COL1A1) in macrophages differentiated from human $CD14^{+}$ peripheral blood monocytes after PMA treatment.** Immunofluorescence staining with (**B)** Mts1 (FSP1/S100A4) mouse monoclonal antibody followed by Alexa Fluor® 594 goat anti-mouse secondary antibody (red); (**C)** Cy3-conjugated α-SMA antibody (yellow); **(D)** P4H-β antibody followed by Alexa Fluor® 594 goat anti-mouse secondary antibody (red); **(E)** FITC-conjugated anti-human COL1A1 antibody (green) of PMA-treated cells. Nuclei were stained with 4,6-diamidino-2-phenylindole (DAPI, blue). (a-b) One-week; (c-d) four-weeks; (e-f) eight-weeks and (g-h) twelve-weeks after PMA activation. Cells were visualized in a Leica DMIRE2 fluorescence microscope. (a,c,e,g). Brightfield phase-contrast images merged with fluorescence images (red/yellow/green) and nuclei stained with DAPI (blue). Magnification: X200.

Figure 2. COL1A1, FSP, FAP and α-SMA expression in YFP macrophages after myocardial infarction in LysM($Cre^{/+}$);ROSA26($EYFP^{/+}$) mouse model. Mouse

myocardial tissue sections were stained with **(A)** anti-COL1A1 antibody followed by Alexa Fluor 594 Goat secondary antibody (red); **(B)** anti-FSP1 antibody followed by Alexa Fluor 594 goat secondary antibody (red); **(C)** anti-FAP antibody followed by Alexa Fluor 594 goat secondary antibody (red); macrophages were stained with FITC conjugated anti-GFP antibody (green); (D) anti-α-SMA antibody followed by Alexa Fluor 594 goat secondary antibody (red). Macrophages were stained with FITC conjugated anti-GFP antibody (green); nuclei were stained with 4,6-diamidino-2-phenylindole (DAPI, blue). (a-c) One-week post-MI; (d-f) Six-weeks post-MI. Tissue sections were visualized under Leica DMIRE2 fluorescence microscope after staining. (a,d) Brightfield phase-contrast images merged with fluorescence images: COL1A, FSP1, FAP or α-SMA (red), macrophages (green) and nuclei (blue); (b,e) merged images (red plus green; arrows point to co-positive cells red+green); (c,f) fluorescent image of the indicated probe (red). Magnification: X200.

Fig 3. Macrophage depletion and inhibition of glutaminase and PFKFB3 to evaluate the role of the resident and infiltrating macrophages after myocardial infarction. Sham mice (n=2) were treated with DMA (dimethylacetamide; vehicle used to dissolve C968 and 3PO) for 3 consecutive days. (**A**) Animals were treated with clodronate liposomes to remove resident macrophages (n=4; administered 1 day prior to MI); treated with the selective inhibitor of glutaminase C968 (n=4; treated with C968 for 3 consecutive days after MI); treated with the selective inhibitor of PFKFB3 3PO that attenuates glycolysis in pro-inflammatory macrophages (n=4; treated for 3 consecutive days after MI). Hearts were processed 1-week post-MI for immunostaining. 5-µm transverse sections were stained with anti-Mac3/CD107b and anti-collagen type I secondary antibodies were Alexa Fluor 488-conjugated goat anti-rat and Alexa Fluor 546-conjugated goat anti-rabbit. Nuclei were stained with DAPI. Images were acquired with an inverted confocal microscope (Metazeiss LSM 710, Plan-Apochromat 40x/1.3oil dic m27) and analyzed using ImageJ. (**B-E**) functional

cardiac parameters at one week after MI: The PR interval (ms) exhibited minimal, but statistically significant higher values in animals depleted of macrophages or treated with 3PO. No differences among animal treatments after MI were observed in the QRS value, in the heart rate, in the ratio of peak velocity of blood flow (E/A ratio) and in the left ventricular ejection fraction (LVEF). *p<0.05 *vs.* DMA

Figure 4. (A) Heart-derived cell populations analysis by flow cytometry. Sham (n=8) and infarcted (n=9) mice were sacrificed and, after digestion of the heart, isolated cells were labeled for CD90, F4/80 and MHC antigens. (**a**) Representative scatter plots. (**b**) The overall cell percentage for each cell population is shown. A restrictive Side Scatter Pulse Height threshold was applied in order to appreciate the minority cell populations. **(B) Expression of macrophage/fibroblast cell markers in CD90$^+$F4/80$^+$ cells.** Cells were labeled as previously indicated and the CD90$^+$F4/80$^+$ populations were sorted and aliquoted. **(a)** Representative plots of sorting. **(b)** Quantitative PCR analysis of *Klf4, Cd163, Cd68, Ly6c, Csfr1, Myhii, Vcl, Tagln, Vim, Tnc, Ddr2* and *Pdgfrb* mRNA expression from sham and infarcted mice (n=8 and 9, respectively). **(c)** Representative immunoblots of the protein levels of CD163, vinculin, transgelin and tenascin-C of the sorted cells. mRNA amounts were normalized to m*36b4* expression (means ± SEM). Pooled samples of protein from sham of MI sorted cells were analyzed by immunoblots (2-3 samples in each lane). Blots were normalized for GAPDH content. Bars indicate mean ± SEM. Student's t-test, *p<0.05, **p<0.005, ***p<0.001.

Graphical Abstract

A. Heart infiltrating myeloid cells from LysM(Cre$^+$);ROSA26(EYFP$^+$) after myocardial infarction acquire a myofibroblast-like phenotype

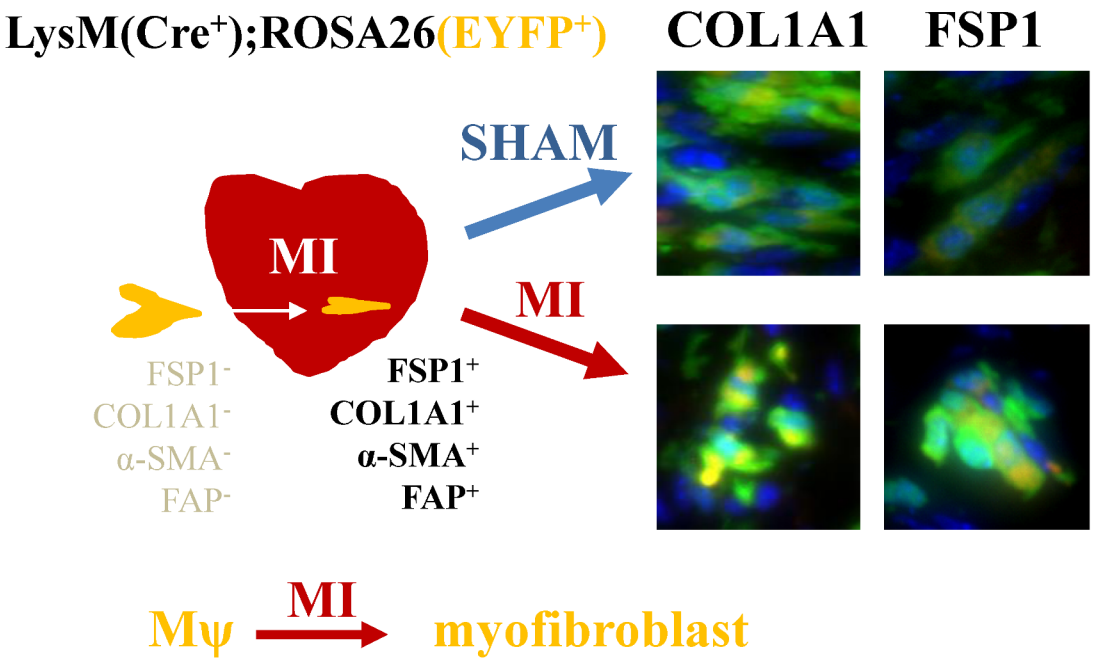

B. Macrophage depletion after clodronate liposomes administration reduces the percentage of Mac3/COL1A1 double positive cells in the heart following myocardial infarction

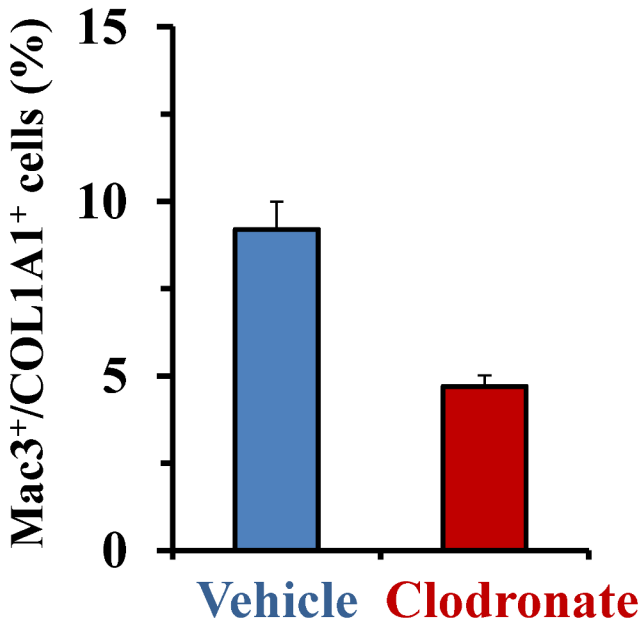

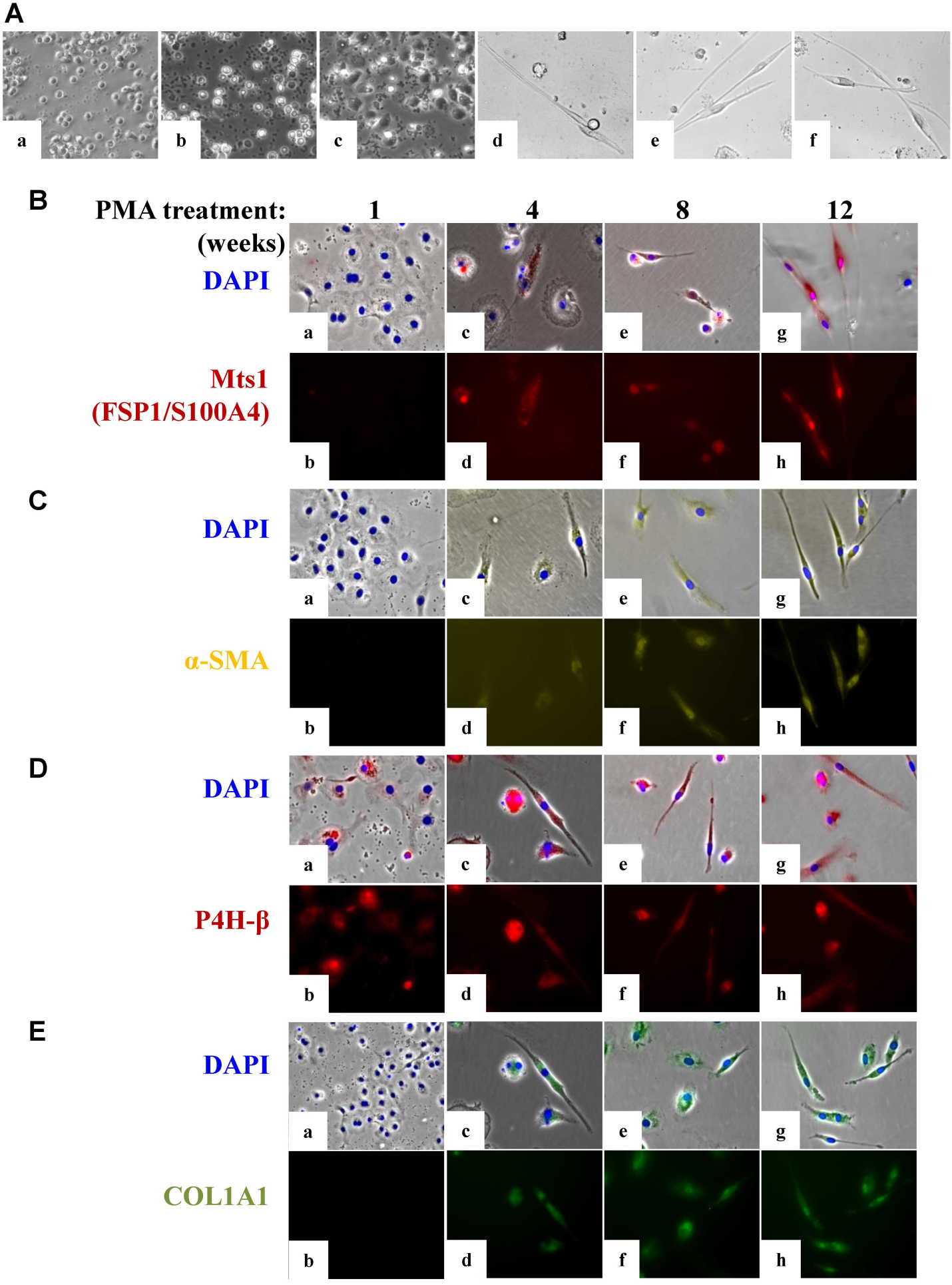
A
a
b
c
d
e
f
B
PMA treatment:
(weeks)
1
4
8
12
DAPI
Mts1
(FSP1/S100A4)
C
DAPI
α-SMA
D
DAPI
P4H-β
E
DAPI
COL1A1

Figure 1

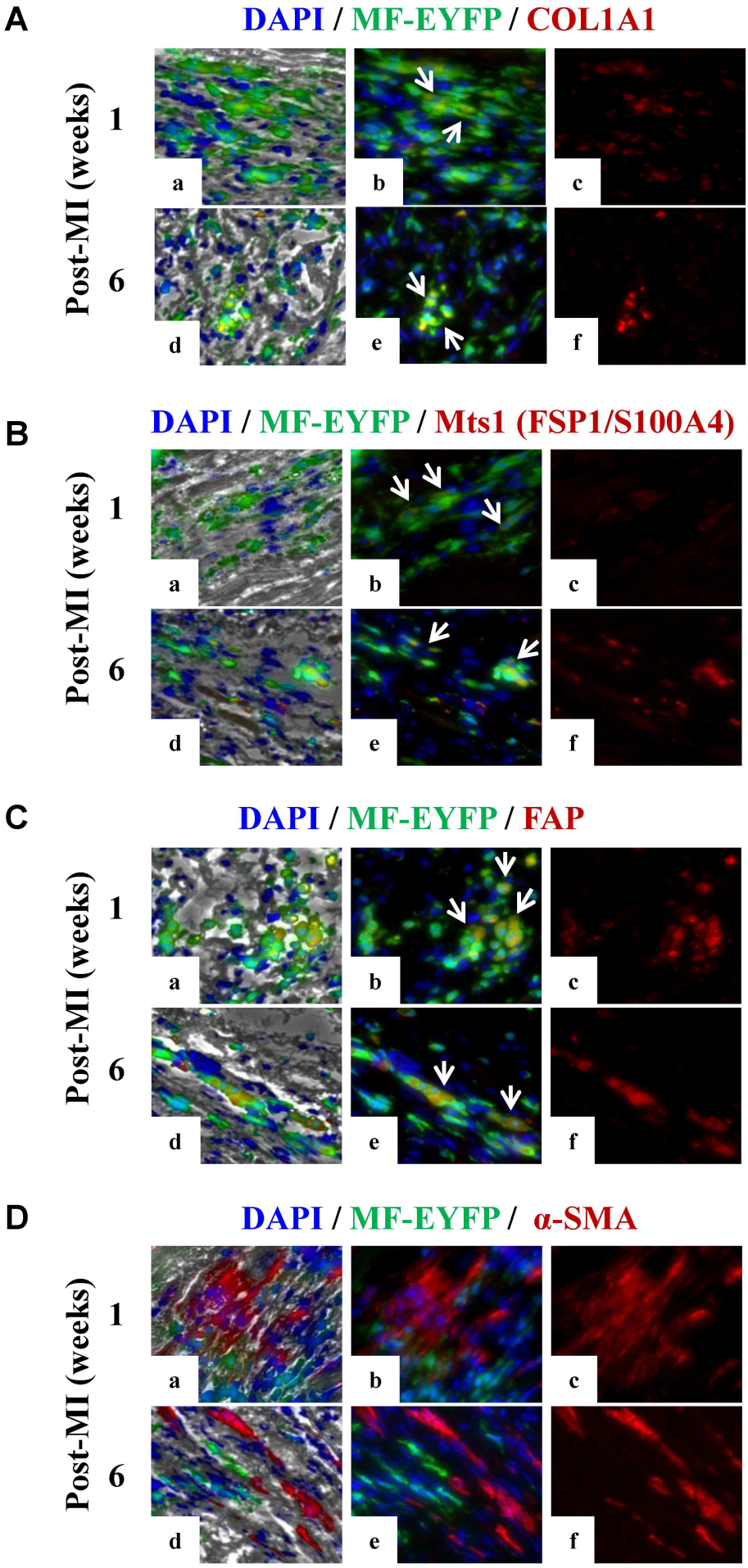
A
DAPI / MF-EYFP / COL1A1
Post-MI (weeks)
1
6
a
b
c
d
e
f
B
DAPI / MF-EYFP / Mts1 (FSP1/S100A4)
Post-MI (weeks)
1
6
a
b
c
d
e
f
C
DAPI / MF-EYFP / FAP
Post-MI (weeks)
1
6
a
b
c
d
e
f
D
DAPI / MF-EYFP / α-SMA
Post-MI (weeks)
1
6
a
b
c
d
e
f

Figure 2

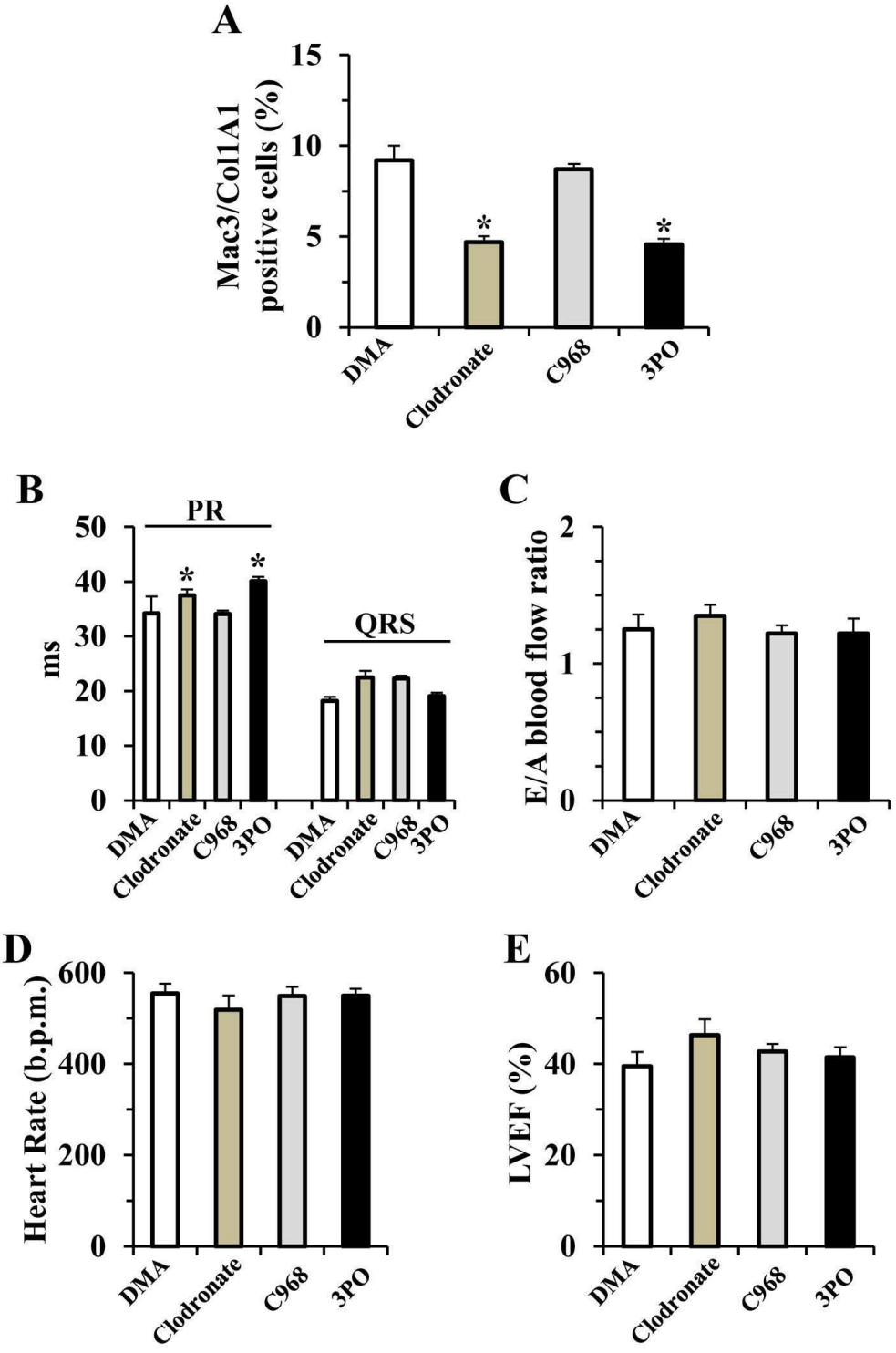
A
Mac3/Col1A1 positive cells (%)
15
10
5
0
*
*
DMA
Clodronate
C968
3PO
B
PR
QRS
ms
50
40
30
20
10
0
*
*
DMA
Clodronate
C968
3PO
DMA
Clodronate
C968
3PO
C
E/A blood flow ratio
2
1
0
DMA
Clodronate
C968
3PO
D
Heart Rate (b.p.m.)
600
400
200
0
DMA
Clodronate
C968
3PO
E
LVEF (%)
60
40
20
0
DMA
Clodronate
C968
3PO

Figure 3

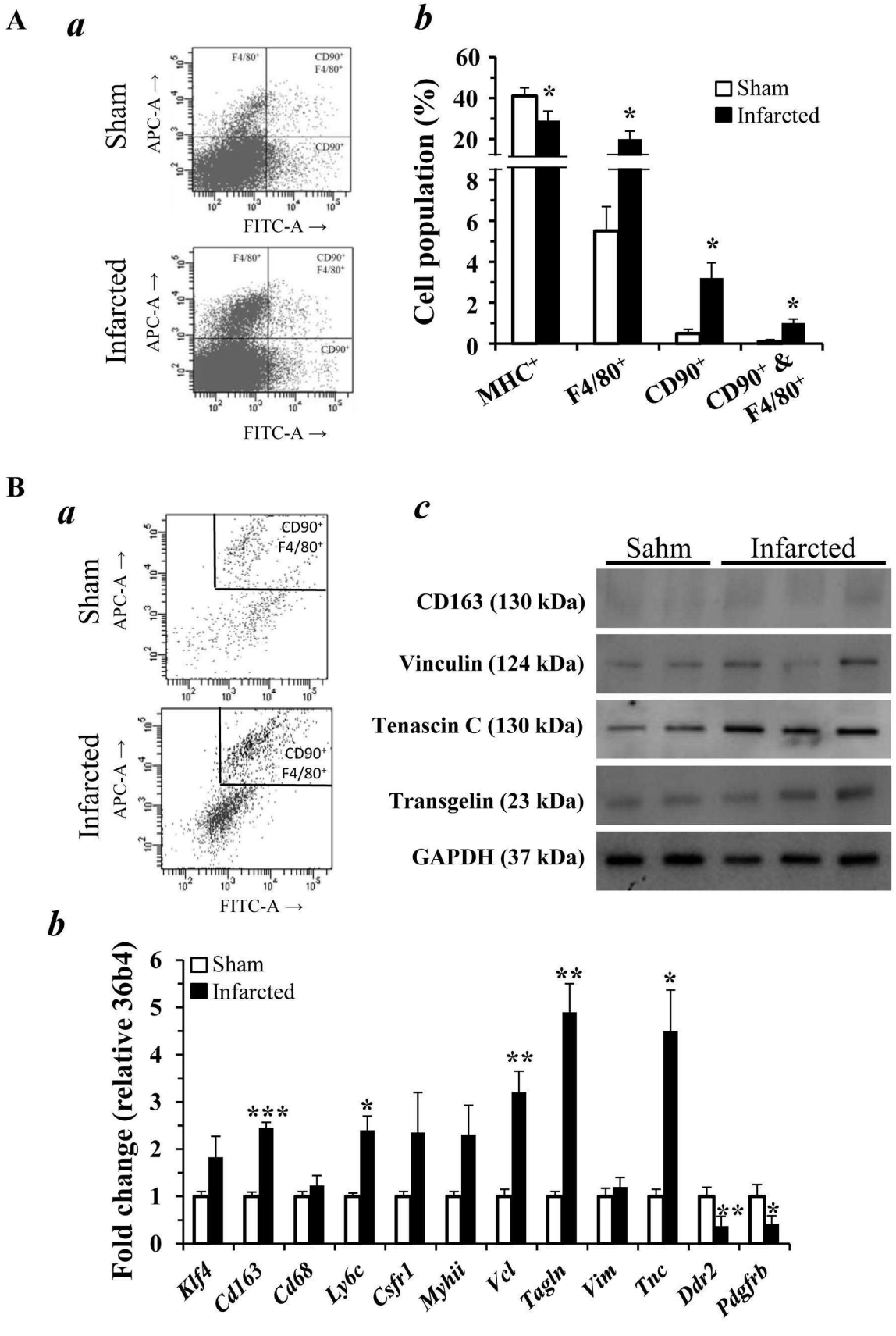
A
a
Sham
Infarcted
APC-A →
FITC-A →
F4/80+
CD90+ F4/80+
CD90+
b
Cell population (%)
Sham
Infarcted
MHC+
F4/80+
CD90+
CD90+ & F4/80+
B
a
CD90+ F4/80+
c
Sahm
Infarcted
CD163 (130 kDa)
Vinculin (124 kDa)
Tenascin C (130 kDa)
Transgelin (23 kDa)
GAPDH (37 kDa)
b
Fold change (relative 36b4)
Klf4
Cd163
Cd68
Ly6c
Csfr1
Myhii
Vcl
Tagln
Vim
Tnc
Ddr2
Pdgfrb

Figure 4

Transition of Macrophages into Fibroblast-like Cells in Healing Myocardial Infarction

Supplemental text:

EXPERIMENTAL PROCEDURES

Antibodies and chemicals. For monocyte isolation Ficoll-Paque PREMIUM (density: 1.077 g/ml) from GE Healthcare Bio-Sciences, Piscataway, NJ was used. $CD14^+$ monocytes were isolated by EasySep Human CD14 Positive Selection Kit from STEMCELL Technologies, Vancouver, Canada. Aldosterone was purchased from Wako Chemicals, Osaka, Japan. Human angiotensin II, phorbol-12-myristate 13-acetate (PMA), 3-(3-pyridinyl)-4-pyridinyl-2-propen-1-one (3PO), 3-Br-4-(dimethylaminophenyl)-2,2-dimethyl-2,3,5,6-tetrahydrobenzophenanthridin-4-one (C968), liposome-encapsulated clodronate and 4,6-diamidino-2-phenylindole (DAPI) were purchased from Sigma-Aldrich, St. Louis, MO. Sircol Collagen Assay Kit was from Biocolor, Newtownabbey, UK. Enhanced chemiluminescence detection kit was purchased from GE Healthcare Bio-Sciences. Primary antibodies, fluorescein (FITC) conjugated mouse anti-human type I collagen, clone 4F6 antibody (Southern Biotech, Birmingham, AL); rabbit polyclonal COL1A1 (H-197) and mouse anti-human Mts1 (X9-7) (FSP1/S100A4) (Santa Cruz Biotech,, Santa Cruz, CA); anti-P4H-β (clone 6-9H6) mouse monoclonal antibody (Acris Antibodies, San Diego, CA); monoclonal anti-α-SMA clone 1A4 Cy3 conjugate and anti-tenascin-C, clone 3B4 (Sigma-Aldrich); anti-GFP antibody (FITC), anti-α-FAP and anti-DDR2 (Abcam, Cambridge, MA); monoclonal anti-transgelin clone C-11 and monoclonal anti-vinculin clone H10 (Santa Cruz Biotech) were used. Secondary antibodies, Alexa Fluor® 594 goat anti-mouse SFX Kit, Alexa Fluor® 488 goat anti-rabbit SFX Kit (Invitrogen, Carlsbad, CA); horseradish peroxidase-conjugated goat anti-mouse or anti-rabbit antibodies (Jackson ImmunoResearch Laboratories, West Grove, PA); anti-GAPDH (Sigma-Aldrich) were used.

Peripheral blood derived CD14$^+$ monocytes. Monocytes were obtained from human peripheral blood buffy coats (each from 50 ml of blood from healthy donors) by Ficoll-Paque centrifugation. Subsequently, CD14$^+$ monocytes were isolated using EasySep Human CD14 Positive Selection Kit, according to the manufacturer's instructions. These cells were grown in RPMI 1640 medium (Mediatech, Manassas, VA) supplemented with 10% fetal bovine serum, 100 units/ml penicillin, 100 µg/ml streptomycin, and 2 mM L-glutamine. Cells were incubated at 1–2x10^6 cells per well in 12 well tissue culture plates for 24 hours at 37°C and 5% CO_2. Finally, CD14$^+$ monocytes were treated with 10 ng/ml of PMA to differentiate monocytes into macrophages. The individual monocyte-derived cultures used in these experiments were obtained from separate donors at different times.

PMA, aldosterone and angiotensin II treatment. Freshly isolated CD14$^+$ monocytes maintained in RPMI 1640 for 24 hours at 37°C (5% CO_2) were treated with 10 ng/ml of PMA to generate macrophages. After 24 h of PMA activation, CD14$^+$ cells were treated with either aldosterone 5 ng/ml, angiotensin II 100 nM or both as indicated.

Cell culture and hypoxia. For hypoxic stress, PMA-treated monocytes with or without aldosterone and angiotensin II were placed in a modular airtight hypoxic chamber (Billups-Rothenberg, Del Mar, CA) with inflow and outflow valves. A preanalyzed air mixture (1% O_2, 5% CO_2, 94% N_2; AIRGAS, Santa Ana, MA) was infused into the chamber to achieve hypoxia. The pO_2 was measured with an oxygen analyzer (Vascular Technology, Nashua, NH) to ensure hypoxia during the entire duration of stress. Cells were maintained in a humidified atmosphere at 37°C for 48 hours.

Immunofluorescence analyses. Cells were fixed with 4% (w/v) paraformaldehyde in phosphate buffered saline (PBS) containing 0.01% Triton x100 for 30 minutes at room temperature (20–22 °C), and washed three times with PBS. Cells were then incubated in blocking buffer [2% (w/v) BSA in PBS] for 60 minutes at room temperature. Fixed and

permeabilized cells were first incubated with FITC-conjugated mouse anti-human type I collagen; monoclonal anti-α-SMA; anti-P4H-β; mouse anti-human Mts1 diluted 1:100 in blocking buffer for 60 minutes at room temperature and washed with PBS to remove unbound antibodies. Cells were incubated with 5 µg/ml of Alexa Fluor® 594-conjugated goat anti-mouse IgG (Invitrogen) for 60 minutes at room temperature following anti-P4H-β and anti-human Mts1 staining. Nuclei were also stained with DAPI (1 µg/ml) for 15 minutes at room temperature. Cells were washed and stored with PBS until visualized. Photomicrographs were obtained with a Leica DMIRE2 fluorescence microscope (×40 objective lens and ×10 eyepiece lens; total magnification, ×400), Hamamatsu C4742-95 digital camera (Tokyo, Japan), and acquisition software Simple PCI Version 5.3.1 (Compix Imaging Systems, Cranberry Township PA).

Preparation of cell extracts. Whole-cell lysates were prepared by lysing cells in lysis buffer (10 mM Tris; pH 7.5, 150 mM NaCl, 1% NP-40, 200 µg/ml leupeptin, 10 µg/ml aprotinin, 1 mM phenylmethylsulfonyl fluoride, 10 mM NaF, 1 mM Na_3VO_4, 1 mM dithiothreitol). Protein concentration was measured using a Bio-Rad DC protein assay kit (Bio-Rad Laboratories, Hercules, CA). Equal amounts of each protein samples for each assay (10-50 micrograms) were separated by 10% SDS-polyacrylamide gels and electroblotted to nitrocellulose membrane by Tran-Blot SD, Semi-Dry Transfer Cell (Bio-Rad). Membranes were then either incubated with rabbit polyclonal COL1A1 antibody, anti-P4H-β mouse monoclonal antibody, anti-tenascin-C antibody, anti-transgelin antibody, anti-vimentin antibody and, after washing, with horseradish peroxidase-conjugated goat anti-mouse or anti-rabbit secondary antibodies. Immunoreactive bands were detected with ECL solution (GE Healthcare Life Sci.) as described (1).

Culture medium of PMA treated CD14$^+$ monocytes. Culture medium of $CD14^+$ monocytes was removed at various time points after activation with PMA and treating with aldosterone,

angiotensin II or both. Five microliters of culture medium of each sample were incubated in loading buffer (125 mM Tris-HCl; pH 6.8, 10% β-mercaptoethanol, 4.6% SDS, 20% glycerol, and 0.003% bromophenol blue), separated by SDS-PAGE, and electroblotted to nitrocellulose membrane. After blocking nonspecific binding sites by overnight incubation in 5% nonfat milk in TBS-Tween (0.05 M Tris-base, 0.9% NaCl, pH 7.6; 0.1% Tween 20), membranes were incubated with the rabbit polyclonal COL1A1 antibody and immunoreactive bands were detected as previously described.

Collagen assay in the culture medium of PMA treated CD14$^+$ monocytes. Culture medium of CD14$^+$ monocytes were removed at various time points after treatment with PMA and assayed for soluble collagen using the Sircol collagen assay, according to the manufacturer's protocol (Biocolor). This assay uses Sirius Red, an anionic dye with sulfonic acid side chain groups, which reacts with the basic amino acids present in collagen. Briefly, Sircol reagent was added to the medium and gently agitated for 30 minutes to allow the collagen–dye complex to form. Collagen–dye complex precipitate was collected by centrifugation at 12,000 r.p.m. for 10 minutes and resolubilized in 0.5 mM NaOH. Absorbance of dye concentration was read at 540 nm by spectrophotometry.

Mice. LysM(Cre$^{/+}$);ROSA26(EYFP$^{/+}$) mice were used to track the fate of macrophages in an MI and heart failure model. LysM(Cre$^{/+}$);ROSA26(EYFP$^{/+}$) mice were generated by crossing the LysM-Cre mouse line (Jackson Laboratory, Bar Harbor, ME; strain 004781) with the R26R-EYFP line (Jackson Laboratory; strain 006148). LysM-Cre mice express Cre in myeloid cells due to a targeted insertion in their endogenous M lysozyme locus. The R26R-EYFP mouse is a Cre-dependent YFP reporter strain (R26R) produced by targeted insertion of EYFP preceded by a loxP flanked (floxed) transcriptional termination sequence (tpA) into the ROSA26 locus. The R26R allele terminates transcription prematurely, but when crossed with LysMCre mice, the Cre-mediated excision of the floxed termination sequence in myeloid cells

leads to YFP expression. LysM($Cre^{/+}$); ROSA26($EYFP^{/+}$) mice are useful for myeloid cell tracking in vivo and exhibit specific and efficient expression of YFP protein in 83–98% mature macrophages and 100% granulocytes (2). In addition to the LysM($Cre^{/+}$);ROSA26($EYFP^{/+}$) mouse strain, two-month-old male wild type mice (C57BL6/J mice; Jackson Laboratory; strain 000664) were used for MI in the same way. When animals were depleted of resident macrophages, clodronate liposomes were administered 2-days prior to MI following the protocol provided by the supplier (Sigma-Aldrich). When animals were treated with inhibitors of glycolysis (3PO) and glutaminase (C968), the drugs were dissolved in dimethylacetamide (DMA) and administered i.p. at 50 mg/kg body weight at day -1, and for 3 consecutive days after MI. Controls received equivalent amounts of DMA. All animal studies were performed in accordance with the NIH Guidelines for the Use of Laboratory Animals and were approved by the institutional and national boards for laboratory animal research.

Experimental MI and heart failure in mice. After anesthesia with intramuscular ketamine (80 mg/kg) and xylazine (15 mg/kg), mice were anesthetized with inhalation of 5% isoflurane and maintained with inhalation of 1-3% isoflurane. Mice were intubated and ventilation was maintained with a Harvard rodent positive-pressure respirator at a respiratory rate of 130/min. Mice were immobilized on a heating pad and subjected to left-sided thoracotomy between the third and fourth intercostal space. MI was induced by permanent ligation of the left anterior descending coronary artery (3). After opening the pericardium, ligation of LAD was made 1 mm under the left atrial appendage using a silk 7/0 suture. MI was confirmed by changes of the affected area from bright red to pale. The left thorax incision was closed with 6.0 monocryl suture. The small pectoral muscle was moved back to its original place and the skin was closed with 6.0 silk sutures. Sham operated mice underwent a similar surgical procedure except without ligation of the LAD (4). Functional parameters were determined by

echocardiography/electrocardiography (Vevo 2100 System, VisualSonics, Toronto, Canada). One week to eight weeks post-MI hearts were harvested for analysis. The heart rate, the PR and QRS intervals (in milliseconds), the E/A ratio of peak velocity of blood flow from gravity in early diastole (the E-wave) to peak velocity flow in late diastole caused by atrial contraction (the A-wave) and the left ventricular ejection fraction(LVEF) were determined.

Immunohistochemical analysis of myocardial tissue sections. At designated time points, hearts were harvested for histology. At each study, time point hearts were excised and washed with PBS. Hearts were fixed in 4 % paraformaldehyde in PBS followed by 30% sucrose and embedded in Tissue-Tek® OCT compound. Myocardial serial tissue cryosections (5-7 µm) were prepared for immunofluorescence analysis. For immunostaining, tissue sections were rinsed in PBS, unspecific binding sites were blocked with 1 % BSA in PBS for 60 min at room temperature, and primary antibodies (1:100 prediluted in blocking solution) were applied for 1 h at room temperature. For double labeling experiments, sections were washed three times with PBS and the second primary antibody was applied for 1 h at room temperature. Antigen-antibody complexes were visualized using fluorochrome (Alexa 484 and 594)-conjugated secondary antibodies (Invitrogen; prediluted in blocking solution). Photomicrographs were taken using a Leica DMIRE2 fluorescence microscope and Compix digital imaging software.

Morphometric analysis. After immunostaining with different fibroblast antibodies (FSP1/S100A4, α-SMA, FAP, COL1A1), ten high power optical fields (x200) were randomly selected, and the number of positive cells was counted for each channel (green, red) as well as the merged channels (yellow) for each animal.

Cardiac cell isolation. 7 days post-MI, ventricular cardiomyocytes were isolated using standard enzymatic digestion (1,5). Briefly, mice were heparinized (4 U/g i.p.), injected with buprenorphine (0.01 mg/kg), and were anaesthetized 30 min later with sodium pentobarbital

(50 mg/kg). The hearts were excised and suspended on a Langendorff perfusion system, the ascending aorta was cannulated, and retrograde perfusion was initiated. Hearts were perfused for 2–3 min at 36–37ºC with a standard calcium-free Tyrode's solution containing 0.2 mM EGTA, and then for 3–4 min with the same Tyrode's solution containing collagenase type II (Worthington) and 0.1 mM $CaCl_2$. Hearts were removed from the Langendorff system, and the ventricles were chopped into small pieces and gently stirred for 3 min in standard Tyrode's solution containing 0.1 mM $CaCl_2$. Cell suspensions were filtered through a 250 mm nylon mesh, pelleted by centrifugation for 3 min at 20***g***, and suspended in Tyrode's solution containing 0.5 mM $CaCl_2$. Single cell suspensions were prepared by passing the resulting solution through a 70 µm cell strainer. After 400***g*** centrifugation for 5 min at 4ºC, the cell pellet was suspended in a storage solution containing 1 mM $CaCl_2$. Tyrode's solution contained (in mM): 140 NaCl, 4 KCl, 1.1 $MgCl_2$, 10 HEPES (pH7.4), 10 glucose and supplemented with 0.5% fatty-acid free BSA (1,5).

***Flow-cytometry*.** Single cell suspensions were stained for 30 minutes at 4ºC with the indicated antibodies. Cells were the analyzed on a FACSCanto II (BD Biosciences) and leukocyte subsets were defined using FlowJo software (Tree Star, Ashland, OR, USA). Monocytes were identified as APC-F4/80$^+$ (1:10, Bio-Rad), fibroblasts as FITC-CD90.2$^+$ (1:100, Biolegend) and cardiomyocytes as APC-MHC$^+$ (1:10, Miltenyi Biotech). For cell counting, absolute counting beads were used (CountBright^{TM}, Invitrogen,). Cells expressing both CD90.2 and F4/80, were sorted in a FACSVantage SE sorter (BD Biosciences), aliquoted and stored at -80ºC.

Real-time PCR. Total cell RNA was isolated by homogenization in QIAZOL® and eluted in a volume of 15 µl using MinElute® columns. 250 ng of RNA were retro-transcribed using a High Capacity CDNA Reverse Transcription Kit (Life Technologies). Real-time PCR was conducted with SYBR Green in a Fast-Real Time PCR System (Life Technologies). The

Real-time PCR assay was performed with 5ng per well of cDNA and the thermocycling conditions were 95°C for 10 min and 40 cycles of 95°C for 15 s followed by 60°C for 1 min. Calculations were made from measurement of triplicates of each sample. The relative amount of mRNA was calculated with the comparative $2^{-\Delta\Delta Ct}$ method. Gene expression was normalized to *36b4*. Primer sequences are available on request.

***Statistical analysis*.** Results are presented as mean ± SEM. Statistical significance was estimated with Student's t test. Grubbs test was used to determine and discard outliers. Differences with values of $p<0.05$ were considered statistically significant.

REFERENCES

1. Val-Blasco A, Piedras M, Ruiz-Hurtado G et al. Role of NOD1 in Heart Failure Progression via Regulation of Ca(2+) Handling. J Am Coll Cardiol 2017;69:423-433.
2. Abram CL, Roberge GL, Hu Y, Lowell CA. Comparative analysis of the efficiency and specificity of myeloid-Cre deleting strains using ROSA-EYFP reporter mice. J Immunol Methods 2014;408:89-100.
3. Clancy RM, Kapur RP, Molad Y, Askanase AD, Buyon JP. Immunohistologic evidence supports apoptosis, IgG deposition, and novel macrophage/fibroblast crosstalk in the pathologic cascade leading to congenital heart block. Arthritis and Rheumatism 2004;50:173-82.
4. Cuadrado-Berrocal I, Gomez-Gaviro MV, Benito Y et al. A labdane diterpene exerts ex vivo and in vivo cardioprotection against post-ischemic injury: involvement of AKT-dependent mechanisms. Biochem Pharmacol 2015;93:428-39.
5. Fernandez-Velasco M, Prieto P, Terron V et al. NOD1 activation induces cardiac dysfunction and modulates cardiac fibrosis and cardiomyocyte apoptosis. PLoS One 2012;7:e45260.

Online Figure 1

Time-course of collagen accumulation in the culture medium of PMA-treated macrophages. Cells were maintained in culture and at the indicated times collagen accumulation was determined in the culture medium using the Sircol collagen assay and by immunoblot. Results show a representative blot or the mean ± SEM of three experiments.

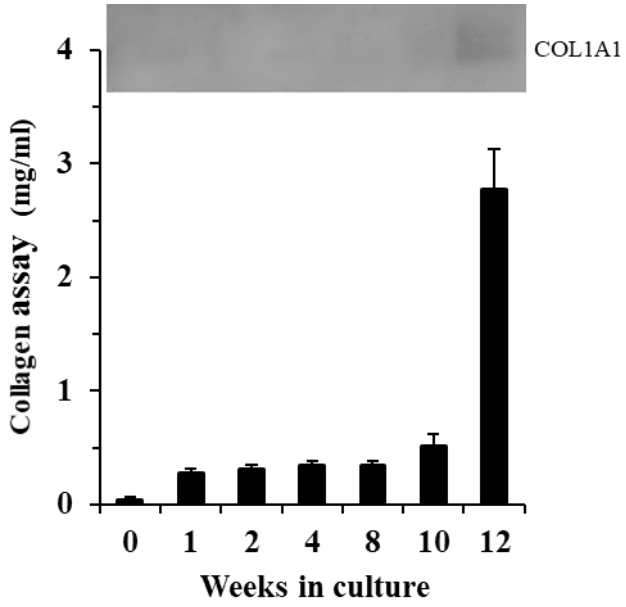

Online Figure 2

Expression of type 1 collagen (COL1A1) in macrophages differentiated from human CD14$^+$ peripheral blood monocytes after PMA, aldosterone and angiotensin II treatment. Immunofluorescence staining with FITC-conjugated anti-human type I collagen antibody (green) of cells treated with PMA for 48 hours followed by aldosterone or angiotensin II or both for 10 days. (a,b) PMA; (c,d) PMA and aldosterone; (e,f) PMA and angiotensin II and (g,h) PMA, aldosterone and angiotensin II. Cells were visualized with a Leica DMIRE2 fluorescence microscope. (a,c,e,g) Brightfield phase-contrast images merged with fluorescence images (green). Magnification: 400X.

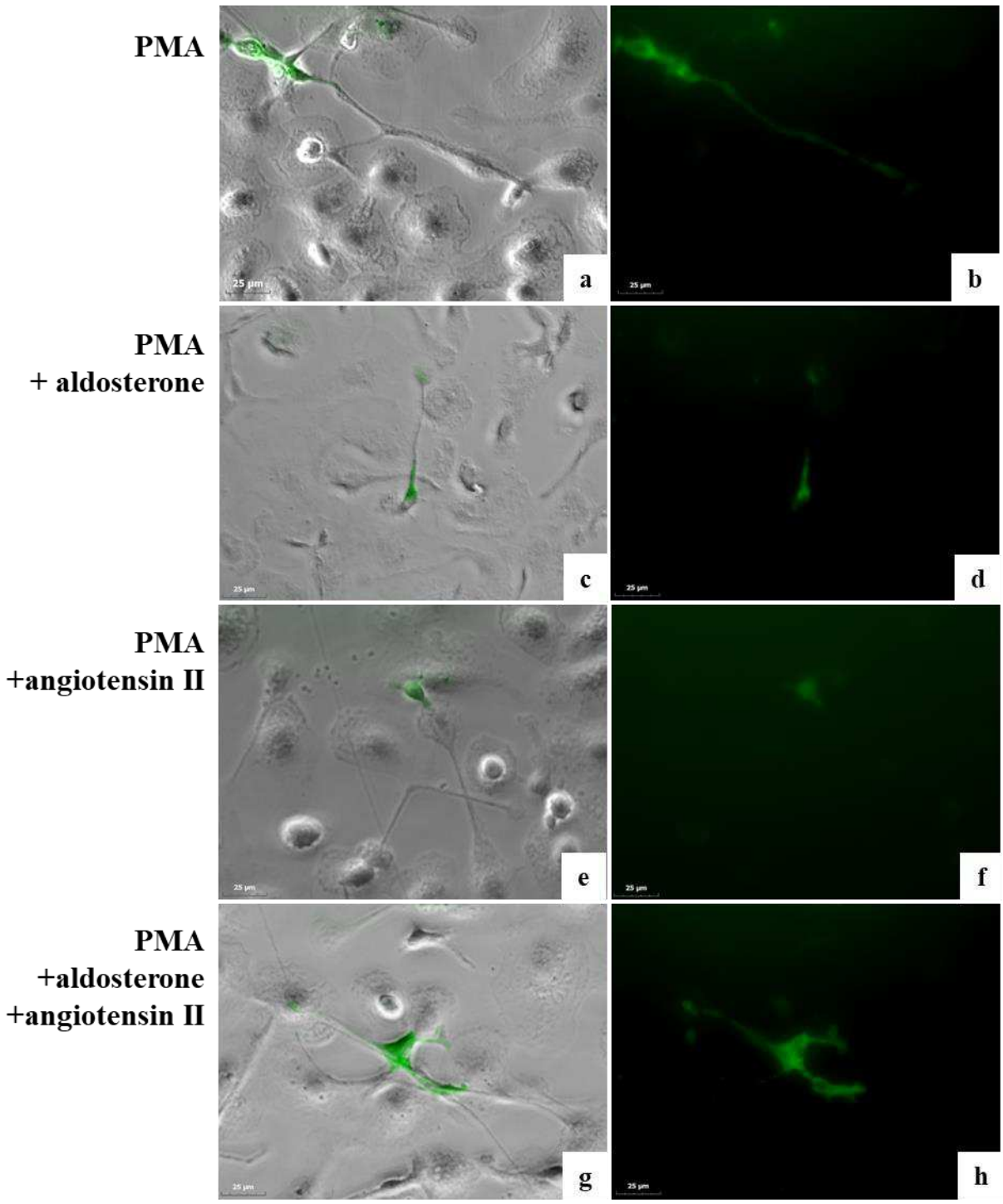
COL1A1
PMA
PMA
+ aldosterone
PMA
+angiotensin II
PMA
+aldosterone
+angiotensin II
a
b
c
d
e
f
g
h

Online Figure 3

Expression of type1 collagen (COL1A1) in macrophages differentiated from human $CD14^+$ peripheral blood monocytes after PMA aldosterone and angiotensin II treatment followed by hypoxic stress. Immunofluorescence cell staining with FITC-conjugated anti-human type I collagen antibody (green); nuclei were stained with 4,6-diamidino-2-phenylindole (DAPI, blue). $CD14^+$ cells were treated with PMA for 48 hours followed by aldosterone or angiotensin II or both for 10 days. Finally these cells were subjected to hypoxic stress for 48 hours (a,b) PMA; (c,d) PMA and aldosterone; (e,f) PMA and angiotensin II and (g,h) PMA, aldosterone and angiotensin II. Cells were visualized in a Leica DMIRE2 fluorescence microscope. (a,c,e,g) Brightfield phase-contrast images merged with fluorescence images (green) and nuclei stained with DAPI (blue). Magnification: 400X.

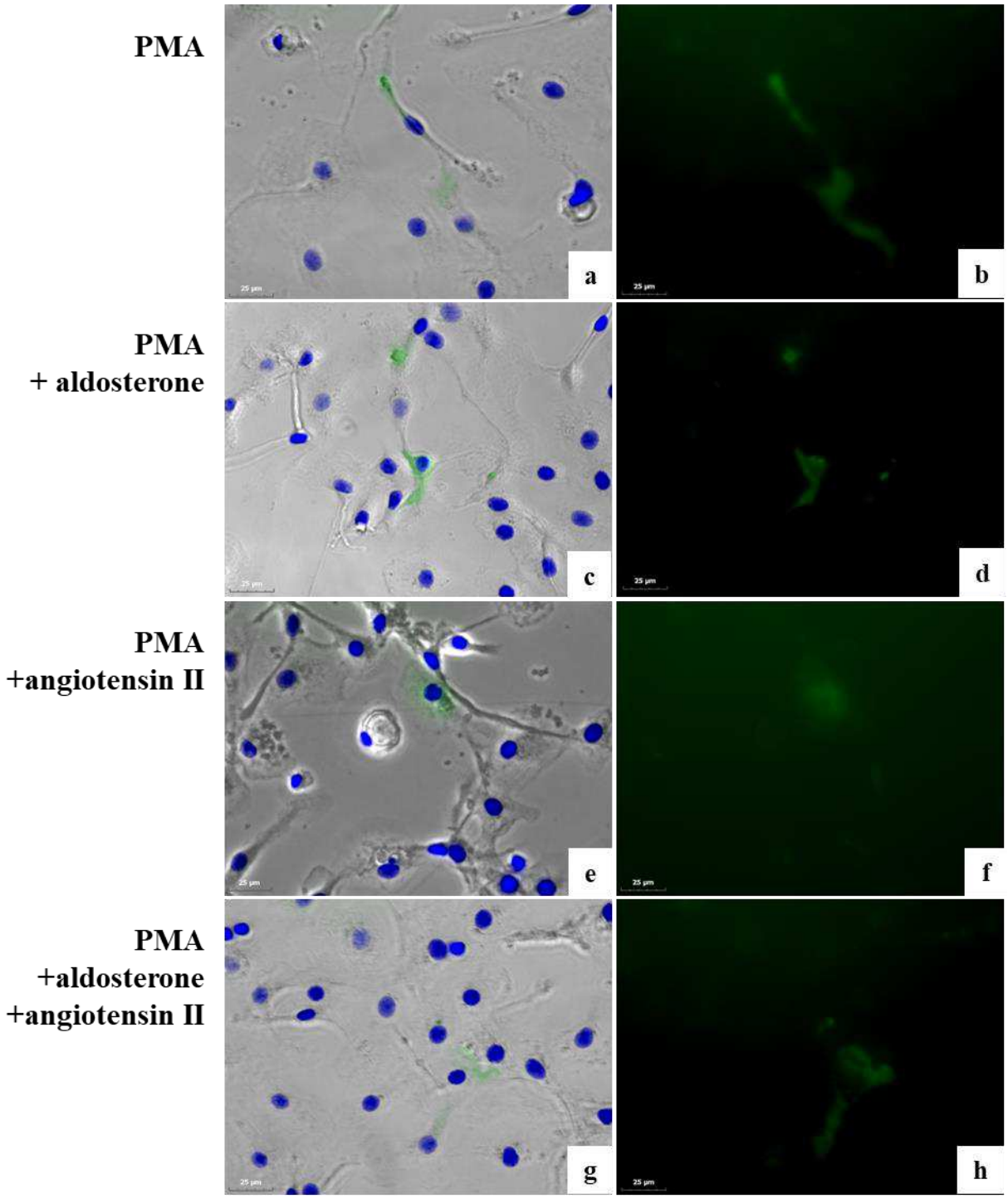
48 h hipoxia → DAPI / COL1A1
PMA
PMA
+ aldosterone
PMA
+angiotensin II
PMA
+aldosterone
+angiotensin II
a
b
c
d
e
f
g
h